



Photo enhanced methanol electrooxidation: Further insights into Pt and TiO₂ nanoparticle contributions

Christopher Odetola, Liliana N. Trevani*, E. Bradley Easton

Faculty of Science, University of Ontario Institute of Technology, 2000 Simcoe Street North, Oshawa, Ontario, L1H 7K4, Canada



ARTICLE INFO

Article history:

Received 19 August 2016

Received in revised form 5 March 2017

Accepted 7 March 2017

Available online 10 March 2017

Keywords:

Glucose

Titanium oxide

Methanol oxidation

Photo radiation

Charge transfer resistance

Electrochemical impedance spectroscopy

ABSTRACT

Pt nanoparticles (PtNPs) were deposited on two different supports: Vulcan® XC-72R carbon (PV) and TiO₂/G-PV, a TiO₂/carbon composite support prepared using glucose-doped Vulcan® XC-72R carbon (G-PV). The presence of TiO₂ has been shown to maximize the PtNPs specific surface area and improves the catalytic performance through Pt-metal oxide interaction. The catalytic activity of Pt/TiO₂/G-PV and Pt/PV toward the methanol oxidation reaction (MOR) was investigated with and without ultraviolet-visible (UV-vis) light irradiation using different electrochemical techniques. The results show the enhancement in catalytic activity in Pt/PV under illumination ($I_{peak\text{ illumination}} - I_{peak\text{ dark}} * 100 / I_{peak\text{ dark}} \sim 100\%$) can be attributed to a significant reduction in the charge transfer resistance (Rct) when the electrode is illuminated (635 Ω (dark) vs 84 Ω (illumination)) as determined by electrochemical impedance spectroscopy (EIS). The observed photo enhancement is relatively modest when compared to the Pt/TiO₂/G-PV catalyst ($I_{peak\text{ illumination}} - I_{peak\text{ dark}} * 100 / I_{peak\text{ dark}} \sim 171\%$), even though the change in the Rct (185 Ω vs. 99 Ω) is not as pronounced as in the Pt/PV samples. The carbon monoxide (CO) stripping results indicate that illumination aids the removal of adsorbed CO from the PtNPs surface. The remarkable enhancement on the oxidation of methanol under UV-vis illumination in the case of the Pt/TiO₂/G-PV catalyst materials show the potential of these materials for applications such as disposable and portable electrochemical sensors for water analysis, mainly the determination of organic contaminants in water. Moreover, it can be a breakthrough in the development of novel photoelectrochemical ethanol sensors and a new generation of energy conversion devices.

© 2017 Elsevier B.V. All rights reserved.

1. Introduction

This paper is aimed to probing some fundamental questions on photo-electrocatalysis driven by UV-vis light on Pt/carbon and Pt/TiO₂/carbon catalyst materials and get further insights on the roles of Pt and TiO₂. The study is centered on methanol oxidation because it is a simple alcohol, and it has been extensively investigated in connection with its use in direct alcohol fuel cells (DAFCs). The thermodynamic equilibrium potential of the methanol oxidation reaction (MOR) is also close to that of the hydrogen oxidation [1] and without recourse to the engineering design challenge of illuminating a fuel cell stack that nowadays seems to be a major limitation, this study can contribute to the development of new generation light assisted energy conversion devices [2]. In addition, the photocatalytic and photoelectrochemical oxidation of

organic pollutants in aqueous media represent two cost-effective approaches for the treatment of pharmaceuticals and industrial waste waters and environment remediation initiatives [3,4].

The methanol oxidation reaction (MOR) on Pt and Pt alloys has been extensively studied in connection to portable fuel cell applications due to their high energy density [5,6]. However, it is still difficult to carry out the complete oxidation of methanol on Pt in acid media, because several reaction intermediates such as formaldehyde, formic acid and most especially carbon monoxide (CO) can be adsorbed on the surface and lead to a rapid deactivation of the Pt catalyst nanoparticles (PtNPs); a main limitation for large-scale applications [7–10].

Significant research efforts have been directed towards these problems over the past several decades. Often Pt-based catalysts have been modified with other metals to maximize performance and reduce the Pt loading [11,12]. In the case of PtRu, one of the best catalysts for the MOR, the reaction proceeds through a bifunctional catalytic mechanism. Pt provides the main site for the dehydrogenation of methanol, and the electrocatalytic performance improves with the oxidation degree of the Ru surface atoms

* Corresponding author.

E-mail addresses: Christopher.Odetola@uoit.ca (C. Odetola), Liliana.Trevani@uoit.ca (L.N. Trevani), Brad.Easton@uoit.ca (E.B. Easton).

since the hydroxide ($-\text{OH}$) groups facilitate the oxidation of CO-like species to CO_2 . However, PtRu catalytic activity is still far from optimal; Ru is also expensive, and its long-term stability during fuel cell operation is a concern [1]. Thus in addition to the search for Pt-alloy catalysts, other studies have involved the exploration of alternative carbon and metal oxide support materials [13–17]. Dispersing catalyst nanoparticles onto metal oxide supports has been shown to enhance both activity and durability for both anodic and cathodic fuel cell reactions. Within this group, TiO_2 is one of the most studied materials, mainly because of its inertness under oxidizing and acidic conditions. It has been used as Pt and Pt-alloy catalyst support for a number of different applications, including the cathode of hydrogen fuel cells and the anode of methanol fuel cells [18]. In the case of the MOR, the presence of a metal oxide can decrease the adsorption energy of CO intermediates and convert them into CO_2 [19]. This enhances surface diffusion of CO to the places where the OH_{ads} partner is formed, thus improving the catalytic efficiency of MOR. However, the low electronic conductivity of metal oxides complicates their usefulness in electrode structure. This, coupled with the challenge of evenly dispersing the metal oxide within the catalysts layer, limits the utilization of catalyst surface area. To overcome these issues, many groups have developed synthetic methods to deposit very thin layers of TiO_2 nanoparticles on carbon. In addition, other groups have prepared catalysts on different types of TiO_x suboxide-modified supports with a higher electronic conductivity [20].

Recently, it has been shown that the electrochemical oxidation of methanol on $\text{Pt}/\text{TiO}_2/\text{C}$ can also be enhanced by illumination with UV light [21,22]. The most commonly accepted mechanism for this process is depicted in Fig. 1. The mechanism involves the creation of holes in the valence band of TiO_2 upon irradiation with UV light, which can enhance the oxidation of methanol molecules and produce a current through the photo-generated electrons [23]. The presence of Pt can suppress recombination of electron-hole pairs and enhance the photocatalytic activity [24,25–27]. Thus, if Pt can be evenly dispersed within the catalysts support, $\text{Pt}/\text{TiO}_2/\text{C}$ has the potential to be a highly active and highly stable photoelectrocatalysts for anodic fuel cell reactions.

In contrast to this, recent studies have shown that the electrochemical oxidation of methanol on Pt/carbon can also be enhanced by illumination with UV light in the absence of TiO_2 . Li and co-workers [28] demonstrated significant enhancement of methanol oxidation on a 40 wt% Pt/C commercial catalyst upon irradiation with UV light. This enhanced activity was attributed to the formation of oxygen-containing species on Pt at lower potentials when irradiated that contribute to the electrooxidation of adsorbed CO [28,29]. A similar improvement in performance has been reported by Arulmani et al. [30] for Pt/C and PtRu/C commercial catalysts for which up to a five-fold enhancement was observed for the electrocatalytic oxidation of methanol when exposed to a broadband source of UV to near infrared light. However, the precise nature of the Pt/C photo-electrocatalysis mechanisms under visible and UV light is still debated. Fig. 1A illustrates another possible mechanism for photoactivation on a Pt/C catalyst for methanol oxidation. In this model, Pt nanoparticles with inherent surface plasma resonance bands in the UV-vis region can absorb UV-vis light and generate high-energy photoelectrons under illumination. The coherent excitation of these free conduction electrons induced by the electrical field of the incident light leaves holes in the inner d band of the Pt metal. The enhanced photochemical reaction takes place by the interaction of the energized charge-carriers from the optically excited nanoparticles and the adsorbed surface reactant molecules [31,32].

Given the fact that a photo enhancement effect occurs with Pt in the absence of TiO_2 , one would reasonably assume that same pathway would also occur in the presence of $\text{TiO}_2/\text{G-PV}$. Further-

more, the presence of electronic interactions between Pt and TiO_2 nanoparticles can alter the electrocatalytic performance (in the absence of irradiation). Together, this leads us to hypothesize that the role of TiO_2 in photo enhancement on $\text{Pt}/\text{TiO}_2/\text{C}$ systems is more complex than initially proposed. For this reason, there is a need to better understand the mechanism of photo enhancement of the MOR in the presence and absence of TiO_2 . To do this, we have prepared a series of Pt/C and $\text{Pt}/\text{TiO}_2/\text{C}$ catalysts and examined their MOR activity in the presence and absence of UV-vis irradiation. The $\text{Pt}/\text{TiO}_2/\text{C}$ catalysts studied here were made using a glucose modification process which controls the morphology and distribution of TiO_2 NPs on pristine Vulcan XC-72R carbon (G-PV) [33,34] so that high utilization of Pt is achieved. We have previously demonstrated that these $\text{Pt}/\text{TiO}_2/\text{G-PV}$ catalysts have improved activity towards the oxygen reduction reaction (ORR) and are highly durable. The pre-adsorption of glucose on pristine Vulcan carbon is a more versatile method to introduce surface functionalities over covalent bonding upon strong acid treatment. This is because the acid treatment approach is often harsh and could induce defects (oxidized surface sites) that may affect the properties of the carbon substrate [35,36]. In addition, this acid treatment approach provides little control over the nature, location, and quantity of the introduced functional groups and also seems to etch carbon surfaces. The use of adsorbed glucose provides an excellent tool to control the size of the deposited TiO_2 particles with homogeneous coating and upon crystallization phase transformation, the glucose carbon will enhance conductivity of TiO_2/C composite. This TiO_2 -modified catalyst used in this study has very similar electrochemical properties (Pt surface area, conductivity) to the Pt/C catalysts studied here, essentially creating an even playing field for comparison of photo enhanced activity.

Electrochemical impedance spectroscopy (EIS) and cyclic voltammetry were used to investigate the MOR on Pt deposited on pristine Vulcan XC-72 (Pt/PV) and Pt supported on 14 wt% TiO_2 /G-doped Vulcan carbon (Pt/ $\text{TiO}_2/\text{G-PV}$). EIS was used to study methanol oxidation and evaluate the charge transfer resistance (R_{CT}) on each prepared catalysts. To the best of our knowledge, this is the first report to examine the R_{CT} for the oxidation of methanol with and without illumination by EIS. These results were analyzed along with those obtained by CO stripping experiments to gain insight into the dominant mechanistic pathways during irradiation.

2. Experimental

2.1. Catalyst synthesis

The as received Vulcan XC72 carbon black (PV) from Cabot Corporation was subjected to glucose doping (G) and TiO_2 deposition through a controlled sol-gel process with subsequent Pt deposition as described in detail elsewhere [33,34]. PV was immersed in a saturated solution of glucose in an ethanol/water solution (80 wt% ethanol). The suspension was centrifuged at 1600 RPM for 15 min and filtered to remove any excess of glucose, and the solid products were dried under vacuum at 60 °C overnight, and the resulting precipitate was oven treated at 80 °C for 3 h. This product is hereafter referred to as G-PV.

A 0.2 M titanium tetrakisopropoxide (TTIP) in isopropanol solution was slowly added with vigorous stirring to a mixture of G-PV in isopropanol. The resulting mixture was refluxed (with stirring) in an oil bath for three hours before the drop-wise addition of 0.2 mL of a water in isopropanol solution. Refluxing of the mixture was continued for an additional 5 h. Subsequently, the resulting mixture was left to stand under continuous stirring for another four days to form a viscous gel. The resultant gel was washed with deionized water until neutral pH and dried in a vacuum oven overnight to

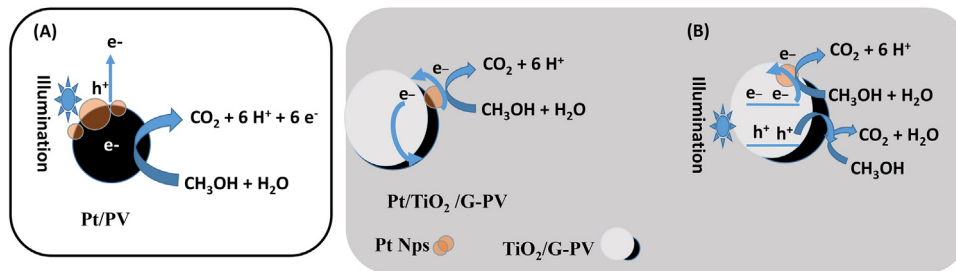


Fig. 1. Schematic mechanism of methanol photo oxidation enhancement on (A) Pt/PV and (B) Pt/TiO₂/G-PV catalysts.

remove moisture content at 80 °C. The dried gel was further heat treated in inert medium at 500 °C for 2 h to promote pyrolysis of glucose carbon and formation of crystalline TiO₂/G-PV composite support.

Pt nanoparticles (avg diam = 5 nm) were deposited on TiO₂/G-PV support using a chemical impregnation method to produce Pt/TiO₂/G-PV catalyst. Pt nanoparticles were also deposited onto PV by the same method to yield the Pt/PV control sample. The average Pt loadings based on thermogravimetric analysis were 16.5 wt% on Pt/TiO₂/G-PV and 22 wt% on Pt/PV (see supplementary information).

2.2. Materials characterization

Thermal gravimetric analysis (TGA) and differential scanning calorimetry (DSC) provided semi-quantitative information about the samples composition and allowed to identify the phase changes and decomposition processes taken place upon heating. These studies were performed using a Q600 SDT Thermal Analyzer from TA Instruments controlled by Q Series software. Samples were heated in alumina pans from room temperature to 1000 °C at a heating rate of 20 °C/min. The atmosphere in the furnace was either extra dry air (Praxair) or argon (99.999%, Praxair) flowing at 50 mL/min. Mass and temperature calibrations were conducted periodically, to ensure a reliable comparison between runs.

Powder X-ray diffraction (XRD) analysis was performed with a Rigaku Ultima IV X-ray diffractometer equipped with a Cu K α X-ray source ($\lambda = 0.154$ nm) was used. Data was collected over a scattering angle range of 10–65° in 0.02° intervals.

X-ray photoelectron spectroscopy (XPS) measurements were performed to determine the surface properties of the catalyst materials. The experimental runs were conducted with a ThermoFisher Scientific K-Alpha (1486.65 eV) system. Charging, if present, was corrected by setting the carbon C 1s peak to a value of 284.6 eV. Data processing and analysis was performed using Advantage 5.926 software.

Transmission electron microscope (TEM) images were acquired using either a JEOL JEM-2010 200 kV high-resolution TEM LaB6 filament or a Philips CM 10 instrument equipped with an AMT digital camera system. Particle size distribution was performed using ImageJ software (Wayne Rasband, Research Services Branch, National Institute of Mental Health, Bethesda, Maryland, USA). HR-STEM micrographs were acquired using an FEI Titan 80–300 cubed TEM (FEI Company, Eindhoven, The Netherlands), operated at 300 kV. The instrument is equipped with a hexapole CEOS image and probe corrector (CEOS GmbH, Heidelberg, Germany). EELS maps were acquired using a Gatan Quantum GIF (Gatan Inc., Pleasanton, CA). The dispersion was set to 1 eV/channel, convergence angle was 19 mrad, and acceptance angle was 36 mrad. Gatan Digital Micrograph was used to extract elemental maps from the raw EELS data cubes.

2.3. Electrode preparation

Catalysts for electrochemical measurements were immobilized on a polished glassy carbon electrode using inks prepared by adding 5 mg of catalyst in a solution containing, 100 μ L of a 5% Nafion® solution and 400 μ L of an isopropyl alcohol/deionized water (50:50 V/V) mixture. After 30 min in an ultrasonic bath, 5 μ L of ink was deposited onto the glassy carbon surface and dried for 5 min. The average Pt loading was $50 \pm 5 \mu\text{g}/\text{cm}^2$ based on this equation:

$$\text{Pt loading } (\mu\text{g}/\text{cm}^2) = \left(\frac{V_C}{V_T} \right) * \left(\frac{\text{Pt content (mg)}}{\text{Glassy carbon surface area}} \right) \quad (1)$$

where V_C represents volume of catalyst on the electrode surface and V_T is the total volume of catalyst solution.

2.4. Electrochemical and photoelectrochemical measurements

Electrochemical experiments were performed in a 50 mL three-electrode cell with an Hg/HgSO₄ reference electrode and a platinum wire counter electrode at 25 °C unless otherwise stated. A factor of 0.650 V was used to convert reference electrode potential to normal hydrogen electrode potential (NHE). The working electrode was a glassy carbon disc electrode (0.196 cm²) that was used to support the catalyst films. Experiments with illumination were carried out in a similar 50 mL glass three electrodes cell with a quartz window and thermostatic jacket (Adams & Chittenden Scientific Glass, PEC Cells 946500.7) and identical reference, counter, and working electrodes.

The light of a 300 W Xenon lamp from a Solar Simulator (XPS-300™) was used for illuminating the working electrode surface and placed less than 5 cm distance away from it. The spectrum of light emitted is flat, with almost equal intensities at all wavelengths throughout the UV and visible ranges. Undesirable heating was avoided with an optical filter at the lamp output for infrared and near-infrared radiation absorption. The power density on the glassy carbon electrode surface was 4.2 mW/cm² as measured with a photometer. Cyclic voltammograms were obtained under nitrogen at a sweep rate of 50 mV/s, including those used for the evaluation of the electrochemical surface area (ECSA) in a deaerated 0.5 M H₂SO₄ solution.

In this work, the surface area of Pt was estimated in two alternative ways: (i) by integration of the area of the hydrogen adsorption/desorption region 0.04–0.41 V vs NHE after correction for double layer capacitance, assuming a monolayer coverage of hydrogen atoms on polycrystalline Pt has a standard charge density of 210 $\mu\text{C}/\text{cm}^2$ and (ii) by CO stripping experiments in a 0.5 M H₂SO₄ solution. For this experiment, CO was pre-adsorbed on the electrode surface at a constant electrode potential (0.15 V vs. NHE) for 20 min. After adsorption, the excess of CO in the solution was removed by purging with N₂. The surface area of Pt was estimated by using the charge density for the oxidation of an adlayer of CO on

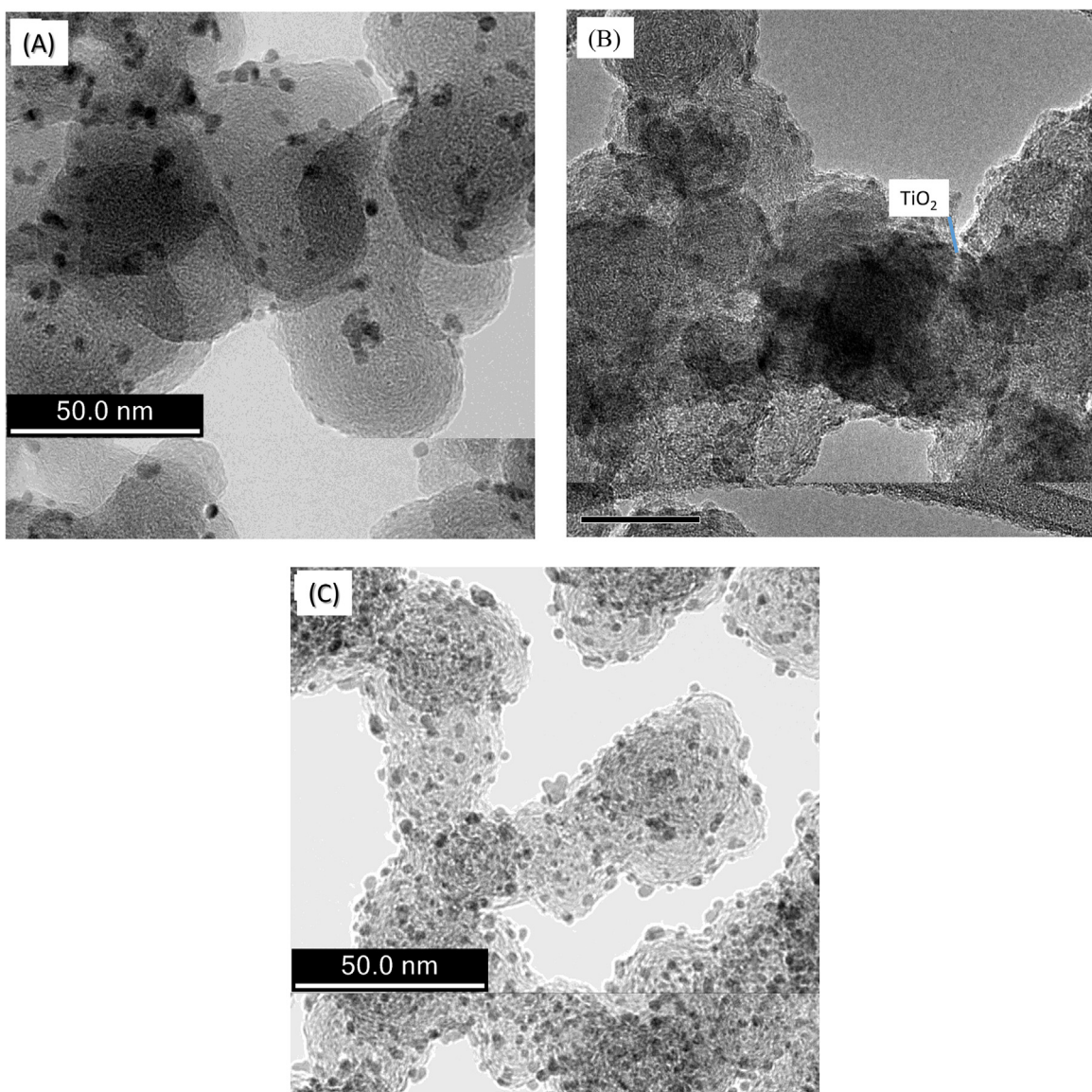


Fig. 2. TEM characterization: (A) Pt/PV, (B) TiO₂/G-PV support, and (C) Pt/TiO₂/G-PV.

Pt to CO₂, 420 $\mu\text{C}/\text{cm}^2$, and taking into account that two electrons are involved in the oxidation reaction [25].

The electrocatalytic activity for the MOR was measured in N₂-purged 0.5 M H₂SO₄ and 0.5 M CH₃OH solutions from 0.3 V to 1.1 V at a sweep rate of 50 mV/s in the presence and absence of light.

The electrochemical studies were performed using a Solartron 1470 potentiostat in combination with a Solartron 1260 impedance analyzer controlled using Multistat 1.1d software (Scribner Associates Inc.) for electrochemical impedance spectroscopy (EIS) measurements. The EIS experiments were conducted from 100 kHz to 0.1 Hz at a DC bias potential of 0.55 V to study the electrochemical oxidation of methanol on the prepared catalysts in the dark and with illumination.

3. Results & discussion

3.1. Physical and chemical characterization of the catalyst materials

Thermogravimetric analysis in air was used to estimate the carbon, TiO₂, as well as the Pt content in the composite catalyst

material. TGA and DSC runs for TiO₂/G-PV support and Pt/TiO₂/G-PV catalyst are shown in Fig. S1. From these plots, residual masses of TiO₂ and Pt catalysts are observed following combustion in air. The Pt loadings in the Pt/PV and Pt/TiO₂/G-PV are given in Table S1.

Fig. 2 shows TEM images of Pt/PV (A) TiO₂/G-PV (B), and Pt/TiO₂/G-PV (C) catalyst materials. In the case of the untreated carbon support (Fig. 2A), the Pt NPs are larger ($4.4 \text{ nm} \pm 1.1 \text{ nm}$) with some aggregation. The reported particle sizes are the average of 200 determinations using the Image J software (Fig. S3). In Fig. 2B, well dispersed TiO₂ nanoparticles ($\sim 10 \text{ nm}$ in diameter) can be seen in the carbon matrix while the small dark particles ($3.4 \text{ nm} \pm 0.7 \text{ nm}$) in Fig. 2C correspond to the Pt nanoparticles on the TiO₂ matrix (bright regions).

The elemental mapping images of the composite support-TiO₂/G-PV and the Pt/TiO₂/G-PV catalyst are shown in Figs. 3 and 4. Fig. 3 allows to clearly identify the support component elements –C, O and Ti that are fairly uniform in agreement with the results of TEM results. In Fig. 4, the elemental mapping images of a Pt/TiO₂/G-PV catalyst sample also confirm the presence of Pt and Ti nanoparticles with minimal segregation on the carbon substrate. The mapping shows that Pt particles are observed in different

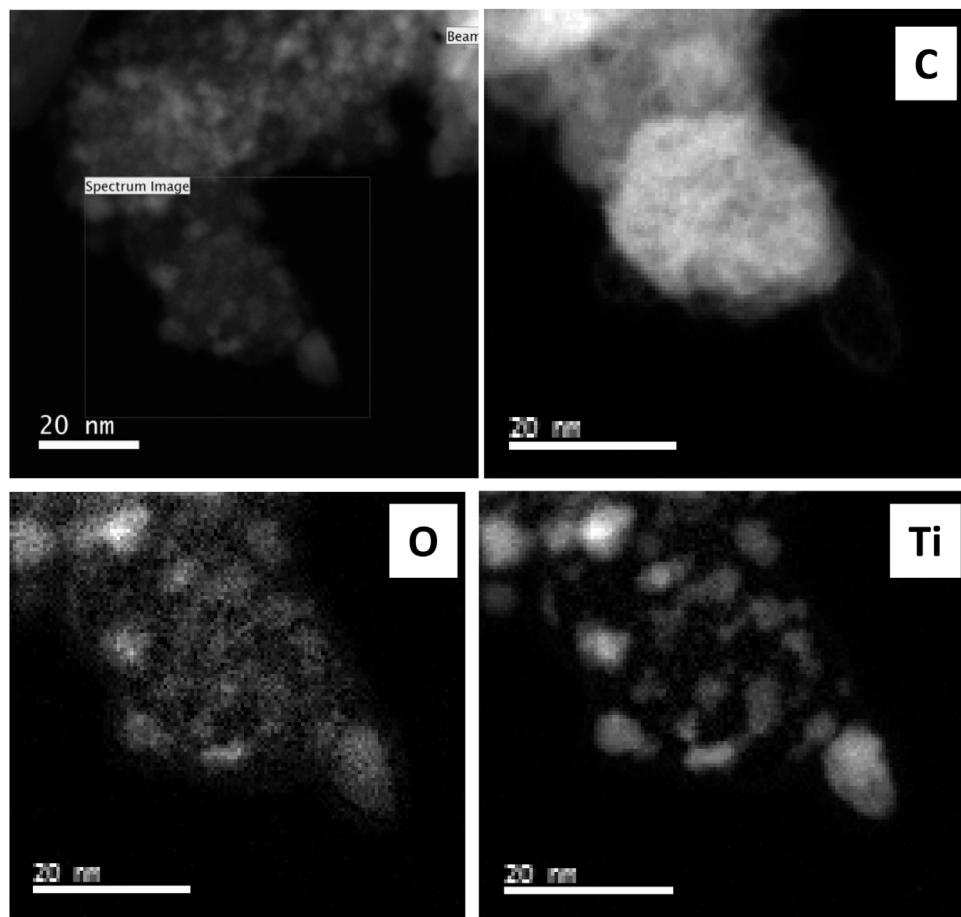


Fig. 3. HR-STEM image of TiO₂/G-PV support and elemental mapping images of C, O and Ti in the sample.

environments, mostly in the TiO₂ nanoparticles region but a few distribution could be observed on uncoated carbon substrate, as well as, at the interface of the TiO₂-C support. Additional, HRTEM images of TiO₂/G-PV supports and Pt/TiO₂/G-PV catalyst (Fig. S4) were obtained in order to ascertain the nanosize distribution of the catalyst components, Pt, TiO₂ and carbon particles.

XRD patterns of PV, Pt/PV, TiO₂/G-PV, and Pt/TiO₂/G-PV are shown in Fig. 5 [33]. The two supports, PV and TiO₂/G-PV, show two broad diffraction peaks at 25° and 43° that correspond to graphitic carbon. Distinct peaks at 27.4°, 36.1°, 41.2°, 54.0°, and 55.0°, due to TiO₂ anatase with Miller indices (101), (103), (112), (105) and (211), along with minor peaks at 33.9° and 37.8° with Miller indices (101) and (200) that correspond to TiO₂ rutile are also observed. Characteristic peaks for fcc Pt are observed on the platinised samples. This is in agreement with our previous finding [33].

XPS was used to evaluate changes in the composition and chemical bonding state of elements at the surface of these materials. As shown in Fig. 6A and B, the O1s spectra of a pure TiO₂ (synthesized) reference sample and the TiO₂/GPV composite support show a major peak at ca. 530.1 eV and 530.0 eV, respectively. A minor peak is observed at higher binding energies ca. 532.3 eV, which arises from TiO₂ and OH functionalities, respectively. The other significant BE peak at 533.92 eV possibly originates from adsorbed H₂O [37]. Fig. S2 shows XPS spectra for Ti (2p) binding energy regions with characteristic peaks of TiO₂ at 458.8 eV (Ti2p3/2) and 464.6 eV (Ti 2p1/2).

Since the surface chemistry of the catalyst support can exert a potential influence on the behavior of the overlying metal NPs, it is of interest to explore the possible metal–support interactions between the PtNPs and the TiO₂ NPs in the catalyst composite mate-

rial. Fig. 6C and D compares the binding energies (BEs) of Pt 4f between the Pt/PV and Pt/TiO₂/G-PV catalysts. The Pt 4f signals for both catalysts were deconvoluted into two pairs of doublets, which can be attributed to metallic Pt (ca. 71.2 eV), Pt (IV) (ca. 73.9 eV), and Pt(II) in PtO or Pt(OH)₂ species (ca. 71.3 eV). The deposition of PtNPs on the TiO₂/G-PV composite support shifted the BEs of Pt 4f to slightly higher values. A positive 0.2 eV shift for Pt/TiO₂/G-PV was detected compared to the Pt/PV catalyst. The shift in the BEs of Pt 4f may be ascribed to the so-called metal–support interactions arising from an increased electron density [38]. This kind of electronic interaction between Pt and the metal oxide support, that shifts the binding energies to higher values with respect to those for the PtNPs has already been reported [39–41]. Moreover, the reduction of Pt is more favorable on TiO₂/G-PV with 86% metallic Pt formed as compared with 76% on Pt/PV.

3.2. Electrochemical activity of the catalyst materials

Cyclic voltammograms (CVs) for the unplatinized support materials in 0.5 M H₂SO₄ are shown in Fig. 7, with and without illumination. The CVs are similar in shape with a distinct peak at ~0.6 V vs. NHE which can be associated with the quinone and hydroquinone peaks. The two supports show considerable currents indicating that they are conductive for electrochemical reactions taken place.

3.2.1. ECSA determination in deareated 0.5 M H₂SO₄ solutions

As described in Section 2.4, CO stripping experiments were used to determine the surface area of the supported PtNPs. The calculated ECSA of Pt/TiO₂/G-PV is 50.9 ± 3.6 m²/g, which is

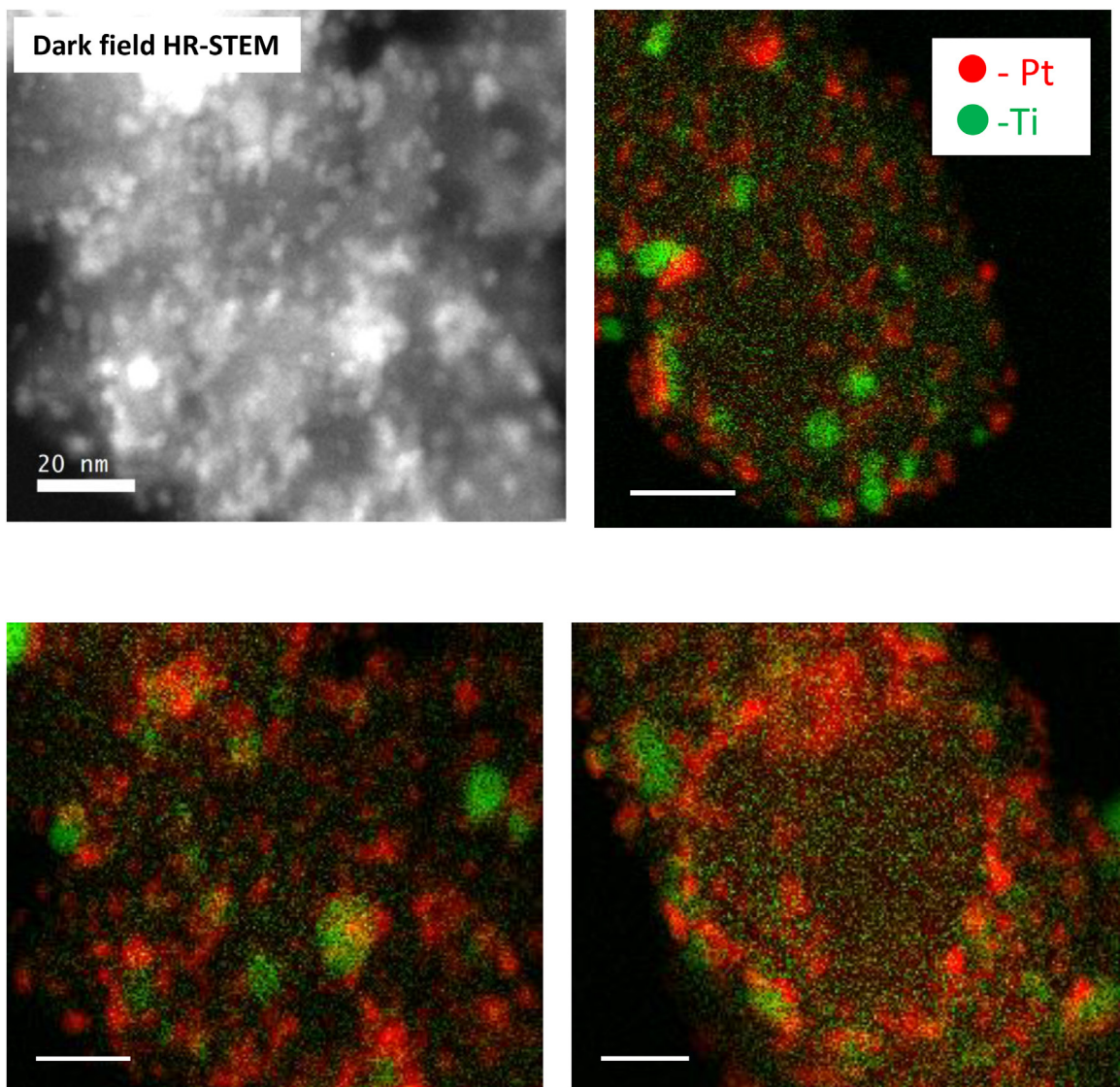


Fig. 4. HR-STEM image of Pt/TiO₂/G-PV catalyst and elemental mapping of Pt and Ti nanoparticles.

remarkably high for an electrode with 14 wt% TiO₂ and comparable to $43.3 \pm 3.2 \text{ m}^2/\text{g}$, obtained for the Pt/PV catalyst. Enhancement of the ECSA for Pt/TiO₂/G-PV may be due differences in Pt particle size as shown in Fig. S3 ($4.4 \pm 1.1 \text{ nm}$ for Pt/PV and $3.6 \pm 1.4 \text{ nm}$ for Pt/TiO₂/G-PV) and a more uniform dispersion of Pt nanoparticles with minimal particle aggregation as observed in the TEM micrograph in Fig. 2C that it can be ascribed to the effect of electronic interaction of Pt on TiO₂ nanoparticles as shown by the positive shift of Pt 4f (Table 1).

3.2.2. Photo-Electrocatalytic activity toward methanol oxidation with and without illumination

Fig. 8 shows the MOR activity of PV, TiO₂ and TiO₂/G-PV support with and without illumination as a control experiment. The bare TiO₂ has negligible electrocatalytic ability toward methanol oxidation. A slight increase in methanol oxidation current was observed under illumination at $\sim 0.70 \text{ V}$. This is not unexpected for a semiconductor material, but electron-hole recombination will be more favorable in samples without PtNPs. The unplatinized supports (PV and TiO₂/G-PV) were also evaluated for methanol oxidation (Fig. 8A and C). Higher capacitive currents were obtained in the presence of methanol on these more conductive supports compared with

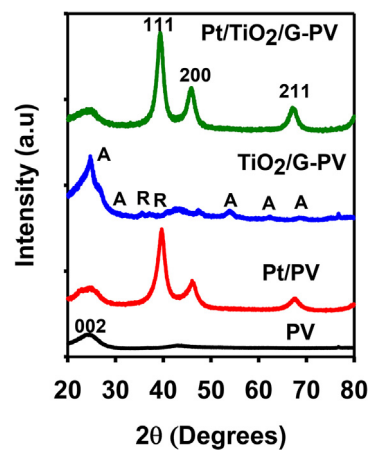


Fig. 5. Powder XRD data for (from bottom to top): PV, Pt/PV, TiO₂/G-PV (A: anatase and R: rutile), and Pt/TiO₂/G-PV catalyst.

bare TiO₂. For the TiO₂/G-PV, a slightly higher current density was observed when compared with PV support. Overall methanol oxidation activity on these supports is low.

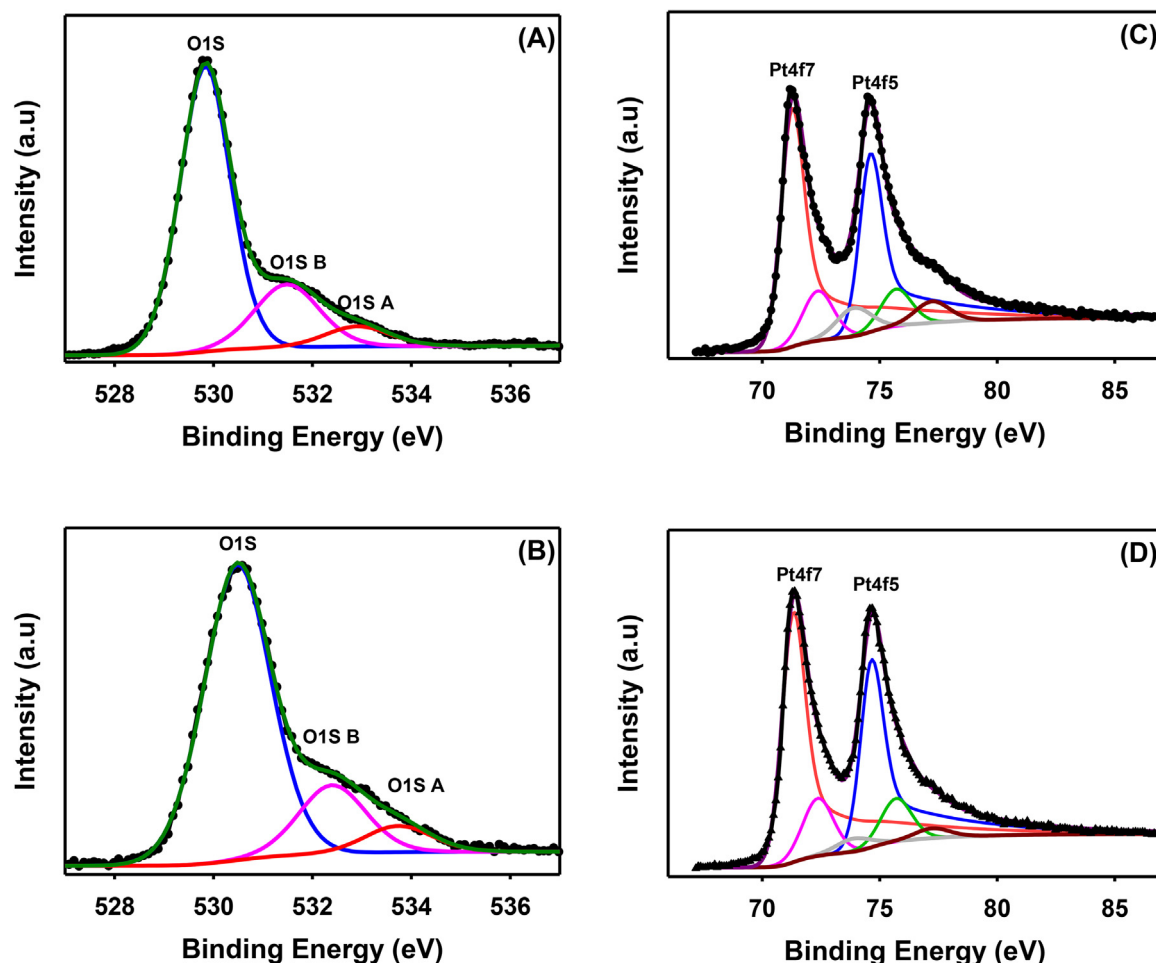


Fig. 6. XPS characterization results. High resolution spectra of O1s for (A) TiO₂, (B) TiO₂/G-PV catalyst supports. High resolution spectra of Pt4f for (C) Pt/PV and (D) Pt/TiO₂/G-PV. Experimental data are represented by symbols.

Table 1
XPS data for reference materials, Pt/PV and Pt/TiO₂/G-PV catalysts.

Catalyst	Species	Binding Energy (eV)	% Composition
	Pt (0)	71.2	75.7
Pt/PV	Pt(II)	72.4	13.6
	Pt(IV)	73.5	10.7
	Pt (0)	71.4	85.6
Pt/TiO ₂ /G-PV	Pt(II)	72.4	10.4
	Pt(IV)	73.7	4.0
	Pt (0)	71.5	64.3
Pt/CNT-TiO ₂ Ref [41]	Pt(II)	72.6	18.7
	Pt(IV)	74.3	17.1
750 Pt/TiO ₂ /C (2:1) Ref [42]	Pt (0)	71.1	77.0
	Pt(II)	72.6	23.0

The MOR activity of the platinized samples (Pt/PV and Pt/TiO₂/G-PV) was investigated. The CV curves, with and without illumination, are shown in Fig. 9. The fact that the maximum currents densities (I_{max}) normalized by either Pt mass or ECSA do not show any significant difference trend between samples rules out Pt utilization as the reason for the enhanced activity. The normalized currents for the Pt/PV and Pt/TiO₂/G-PV samples start to increase at ~ 0.46 V vs. NHE for both dark and under illumination. The shape of the curves for the forward process are also similar to each other. The moderate enhancement observed under illumination in the case

Table 2
Total peak current density and current contributions for methanol oxidation at 0.8 V vs NHE with and without illumination.

Sample	Illumination $I_{total-forwardmax}$ (A/g Pt)	Enhancement ^a
Pt/PV	No	678
	Yes	1357
Pt/TiO ₂ /G-PV	No	1214
	Yes	3293
Pt-TiO ₂ /C (Ref. [38])	No	1043
	Yes	2597

^a $(I_{total-forwardmax(\text{light})} - I_{total-forwardmax(\text{dark})}) * 100 / I_{total-forwardmax(\text{dark})}$.

of PtNPs deposited on a carbon substrate, Pt/PV, is quite interesting, and it was found in the past by other groups [28]. However, the presence of TiO₂ on G-PV clearly leads to a greater enhancement in photoelectrocatalytic activity. The total current density for the MOR and the enhancement observed under illumination, $(I_{total-forwardmax(\text{light})} - I_{total-forwardmax(\text{dark})}) * 100 / I_{total-forwardmax(\text{dark})}$, are summarized in Table 2.

In the absence of illumination, the forward peak current density on Pt/TiO₂/G-PV for methanol oxidation (1214 A/g Pt) is 1.8 higher than that of Pt/PV (678 A/g Pt). The presence of TiO₂-OH surface groups on Pt/TiO₂/G-PV will facilitate the MOR even in the absence of light [42], because the oxidation kinetics of CO and other intermediate oxidation species formed during MOR is governed by the binding strength of adsorbed CO and presence of OH functional

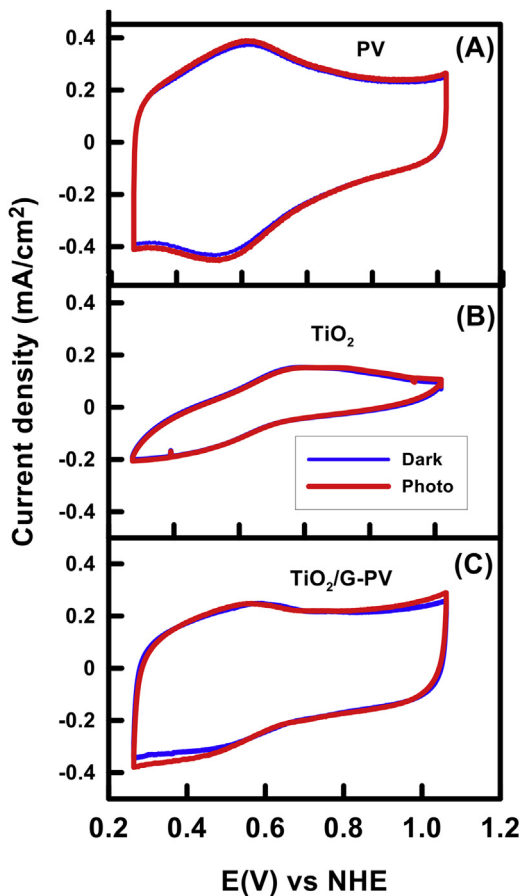


Fig. 7. Cyclic voltammetry of unplatinized supports: (A) PV, (B) TiO_2 (homemade) and (C) $\text{TiO}_2/\text{G-PV}$ carried out in nitrogen saturated $0.5 \text{ M H}_2\text{SO}_4$ at 25°C and 50 mV/s scan rate. Currents normalized by the GC electrode geometrical area = 0.196 cm^2 .

group on the metal surface [43]. The results are in good agreement with the behavior reported for PtNPs deposited on carbon and carbon-coated TiO_2 fibers [44], despite the fact that in these cases the PtNPs are not in direct contact with TiO_2 , but on a mesoporous carbon film.

In the presence of UV-vis light illumination, the enhancement observed for the oxidation of methanol on $\text{Pt}/\text{TiO}_2/\text{G-PV}$ ($3293 \text{ A/g}_{\text{Pt}}$) is 2.4 times higher than that of Pt/PV ($1357 \text{ A/g}_{\text{Pt}}$). Thus, the intrinsic photocatalytic activity of TiO_2 and surface area effect of the composite support promotes overall a significant enhancement in electrocatalytic activity. Also, the formation of O-containing species on Pt under illumination on the Pt/PV catalyst at lower potentials can facilitate electrooxidation reaction of adsorbed CO intermediate formed [28].

Chronoamperometry with intermittent illumination in repeated off-on cycles was used for studying the contribution of the photocurrent to the current density. These curves were obtained by polarizing the electrodes at 0.85 V . As shown in Fig. 10, with the light off, a remarkable decrease in current density can be observed in the polarization curves for the repeated cycles. The significant enhancement in photocurrents on base metal catalysts and composite catalyst indicates the synergistic effects of the catalyst components following illumination in good agreement with the behavior observed on other $\text{Pt}/\text{TiO}_2/\text{C}$ catalysts [44,45]. In addition, this type of enhancement on metal supported catalyst is comparable to literature data where ~ 3 fold improvement in a photocurrent was observed on Pt/C catalyst using a solar simulator as a light source [28]. This indicates that MOR was improved by irradiation via a photochemical reaction.

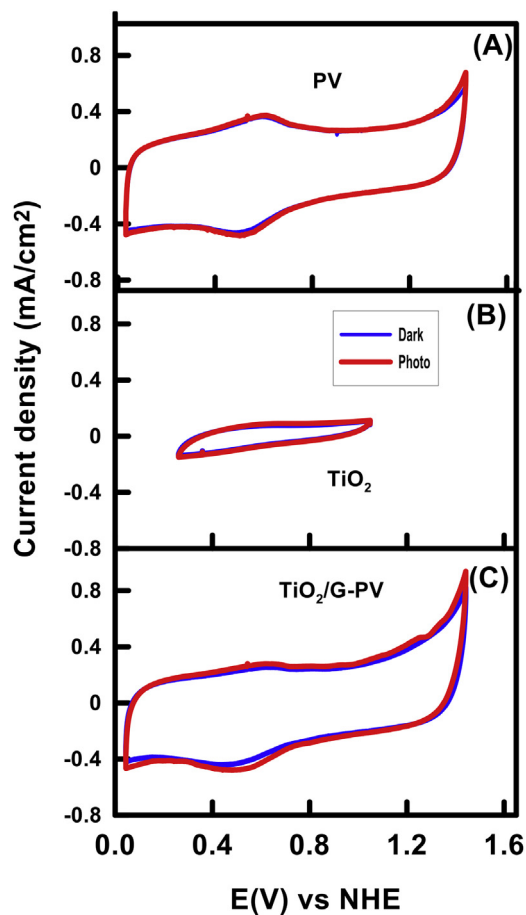


Fig. 8. Methanol oxidation activity at 25°C of (A) PV, (B) TiO_2 (homemade) and (C) $\text{TiO}_2/\text{G-PV}$ supports with and without irradiation in nitrogen saturated $0.5 \text{ M CH}_3\text{OH} + 0.5 \text{ M H}_2\text{SO}_4$ solution at a scan rate of 50 mV/s . Currents normalized by the GC electrode area = 0.196 cm^2 .

However, given the fact that photo-enhancement occurs in the presence and absence of TiO_2 , EIS measurements were carried out to evaluate how charge transfer kinetics of methanol oxidation are altered in the presence of illumination.

An intermediate direct current (DC) bias potential of 0.55 V was chosen to compare the reactivity of prepared catalysts [46] and modeled with an equivalent circuit [47], representing the impedance behavior (Fig. 11). The equivalent circuit (Fig. 11C) includes the solution resistance (R_s) between the working electrode and the reference electrode, a constant phase element (CPE), representing the double layer capacitance of the absorbed methanol, the charge transfer resistance (R_{CT}), inductance (L), related to the methanol dehydrogenation and the intermediates adsorption reactions. The methanol oxidation process at the catalyst interface can be treated as a parallel model of CPE and a resistor (R_2).

The Nyquist plots consist mainly of semi-circles, whose diameters are associated with the charge transfer resistance for MOR [48,49]. The Nyquist plots obtained for each catalyst in the presence and absence of irradiation are shown in Fig. 11(A–B). The expected semi-circle response was observed in all cases, with a clear reduction in the diameter when UV irradiation is present. Each spectrum was readily fit to the equivalent circuit model; the values of R_{CT} obtained from fitting each spectrum are listed in Table 3. The Nyquist plot of Pt/PV catalyst is similar that observed for EIS studies of methanol oxidation on a Pt/C thin film electrode Pt electrode and the resistance of charge transfer is in agreement with literature data obtained at similar potential region [50]. The exchange

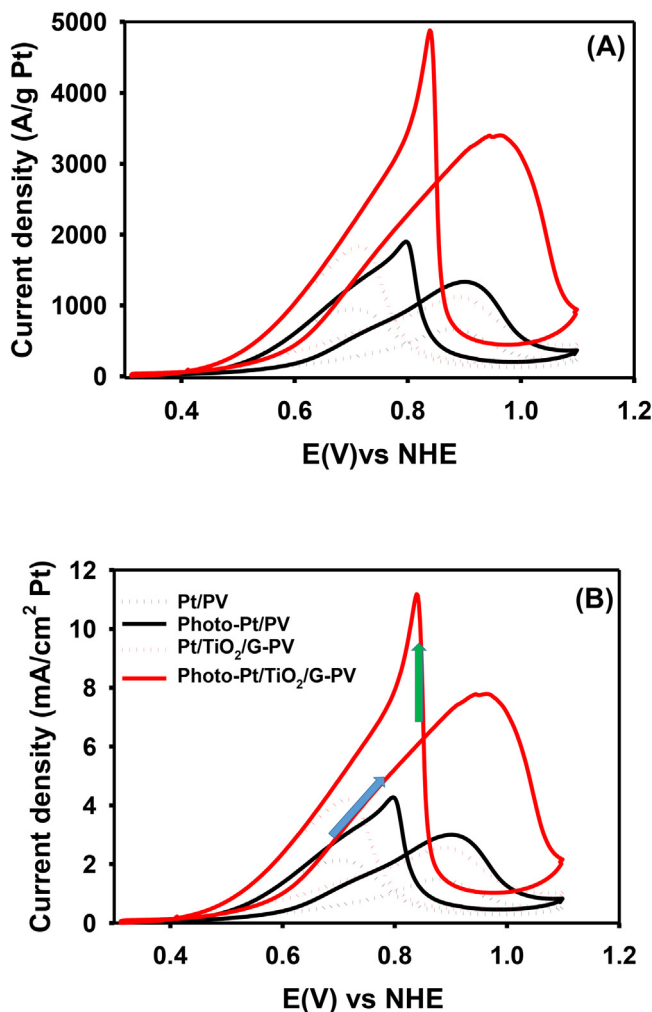


Fig. 9. Methanol oxidation on platinized supports at 25 °C. (A) Mass activity and (B) Specific activity with and without irradiation in nitrogen saturated 0.5 M CH₃OH + 0.5 M H₂SO₄ solution at a scan rate of 50 mV/s.

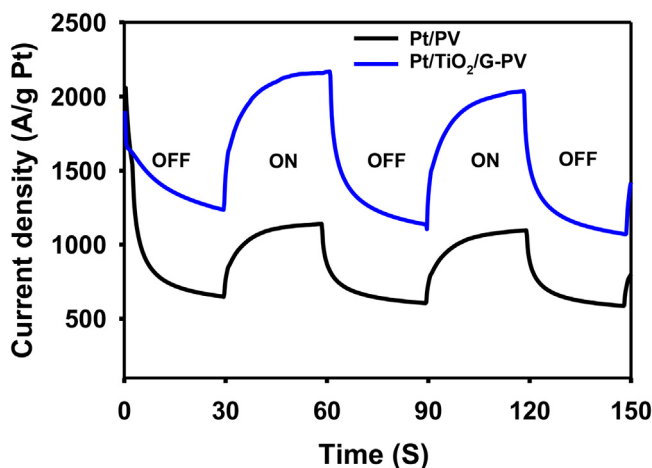


Fig. 10. Chronoamperometry intermittent irradiation of catalyst materials at 25 °C and 0.85 V in nitrogen saturated 0.5 M CH₃OH + 0.5 M H₂SO₄ solution.

current density, j_0 , was determined using the values of R_{CT} and the linearized form of the Butler-Volmer equation [51]:

$$j_0 = \frac{RT}{nFAR_{CT}} \quad (2)$$

Table 3

Charge Transfer Resistance (R_{CT}) at 0.55 V vs NHE and exchange current density (j_0) obtained from EIS data for Pt/PV and Pt/TiO₂/G-PV catalysts.

Samples	R_{CT} (Ω)	j_0 (mA/cm ²)
Without illumination		
Pt/PV	635 ± 10	0.034
Pt/TiO ₂ /G-PV	185 ± 9	0.12
With illumination		
Photo-Pt/PV	83.6 ± 3.5	0.26
Photo-Pt/TiO ₂ /G-PV	98.7 ± 5.0	0.22
Pt/C (Dark) (Ref [50])	~660 (0.375 V vs Ag/AgCl)	–

where R corresponds to the ideal gas constant, T corresponds to the cell temperature, F is Faraday's constant, A is the geometric area of the electrode (0.196 cm²), and n is the number of electrons transferred in the reaction (n = 6 for MOR).

In the absence of irradiation, R_{CT} was ca. 3-times higher for Pt/PV compared to Pt/TiO₂/G-PV. This indicates that TiO₂ has a favorable influence on MOR kinetics in the absence of irradiation. In the presence of UV irradiation, the charge transfer resistance was considerably lower for each catalyst leading to the observed enhancement in MOR kinetics. However, it is worth noting that the measured value of R_{CT} and j_0 for each catalyst were very similar in the presence of UV irradiation, with the kinetics slightly more favorable on Pt/PV. This striking similarity implies that the photo enhancement should be given by changes in the Pt-CO binding energy and separation efficiency of the photogenerated electron-hole pairs due to surface-plasmon-induced charge separation in PtNPs in contact with TiO₂ [52]. To further understand this phenomenon, we examined the influence of illumination on the activity of each catalyst towards CO stripping.

3.2.3. CO stripping experiments in the presence and absence of UV-vis light

Fig. 12 shows the CO oxidation voltammograms (before and after CO stripping) on Pt/PV and Pt/TiO₂/G-PV catalysts. We observed that illumination leads to a reduction in the onset potential of ca. 40–50 mV for both catalysts, indicating that illumination does indeed alter energetic around CO removal from the Pt surface. The presence of TiO₂ NPs also has a beneficial effect, showing lower onset potentials. This further implies that TiO₂ is also influencing the kinetics of CO removal on the electrode surface. The presence of pre-wave/shoulder on Pt/TiO₂/G-PV catalyst is likely due to the presence of domains of a different surface phase as it was observed in the case of PtRu catalysts [53]. Also, the onset potential of CO_{ad} oxidation for Pt/TiO₂/G-PV (0.78 V) catalyst shifted negatively compared to the Pt/PV (0.85 V) in the dark. This further indicates that a more conductive composite support accelerates the oxidative removal of CO adsorbed on the Pt active sites and was consistent with the results of methanol oxidation and EIS measurements and the higher ECSA of the Pt/TiO₂/G-PV catalyst determined by both H₂ adsorption/desorption and CO stripping experiments.

To rule out any temperature effect on the observed behavior, the CVs of methanol electro-oxidation were recorded at temperatures ranging from 15 to 55 °C with and without illumination. As shown in Fig. 13A and B, the MOR current on Pt/PV and Pt TiO₂/G-PV increase with temperature, but the onset potential and the peak potential did not vary significantly with temperature increase.

The apparent activation energy, E_a^{app} , values for the MOR obtained from the slope of the Arrhenius plots, ln (current) vs 1/T, at several constant potentials (Fig. 13C and D) are summarized in Table 4. It is clear that the potential dramatically affects the E_a^{app} values, thus limiting the comparisons that can be made between different catalyst materials. Nevertheless, at 0.85 V (~peak potential for both samples) and in the absence of irradiation, the E_a^{app} are

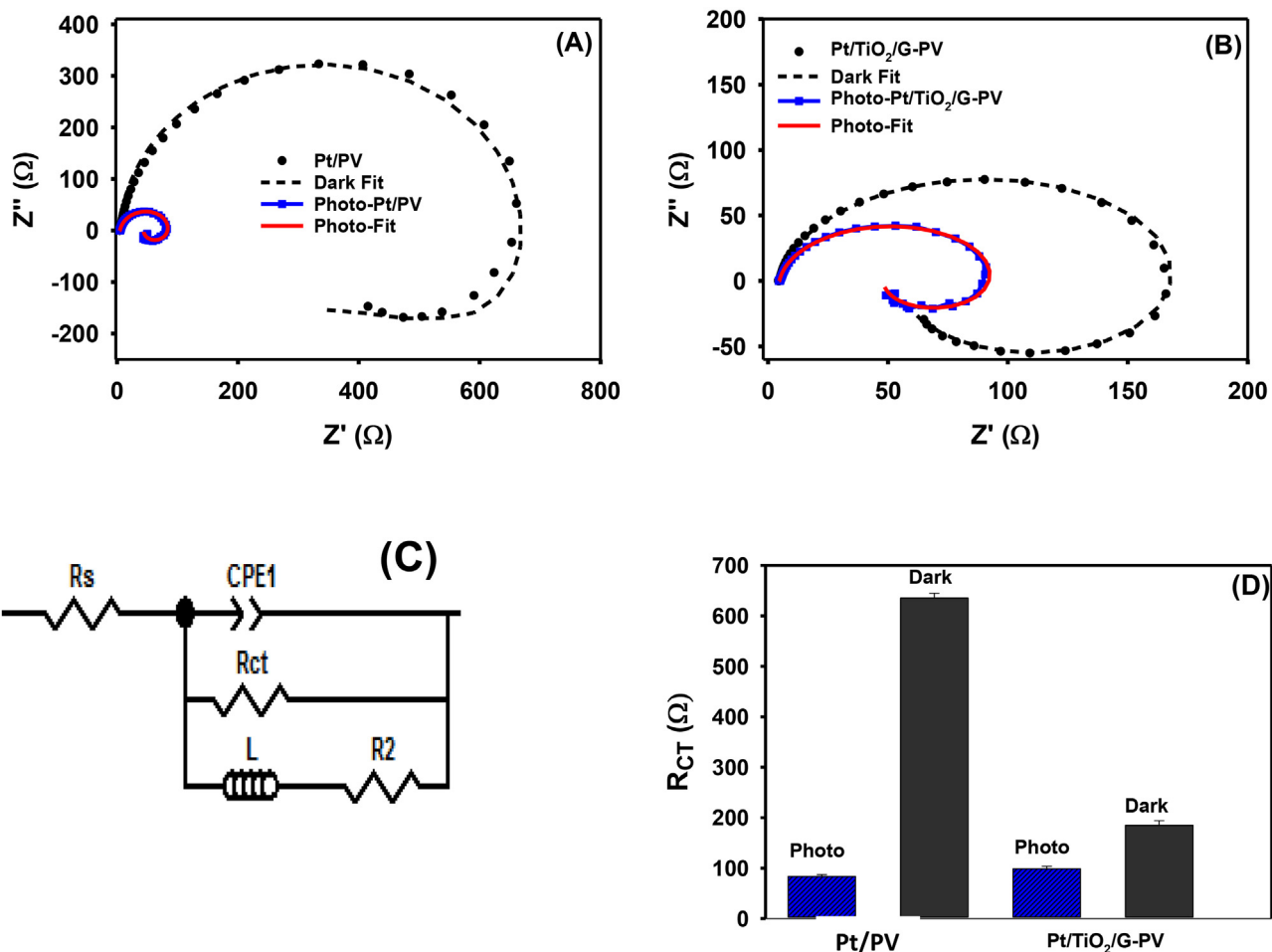


Fig. 11. Nyquist plots at 25 °C and 0.55 V for (A) Pt/PV and (B) $Pt/TiO_2/G-PV$ with corresponding fittings from the equivalent circuit; (C) Equivalent circuit for fitting impedance data, in nitrogen saturated 0.5 M $CH_3OH + 0.5 M H_2SO_4$ solution; (D) Charge transfer resistance with and without irradiation from fitting impedance data to the equivalent circuit (C).

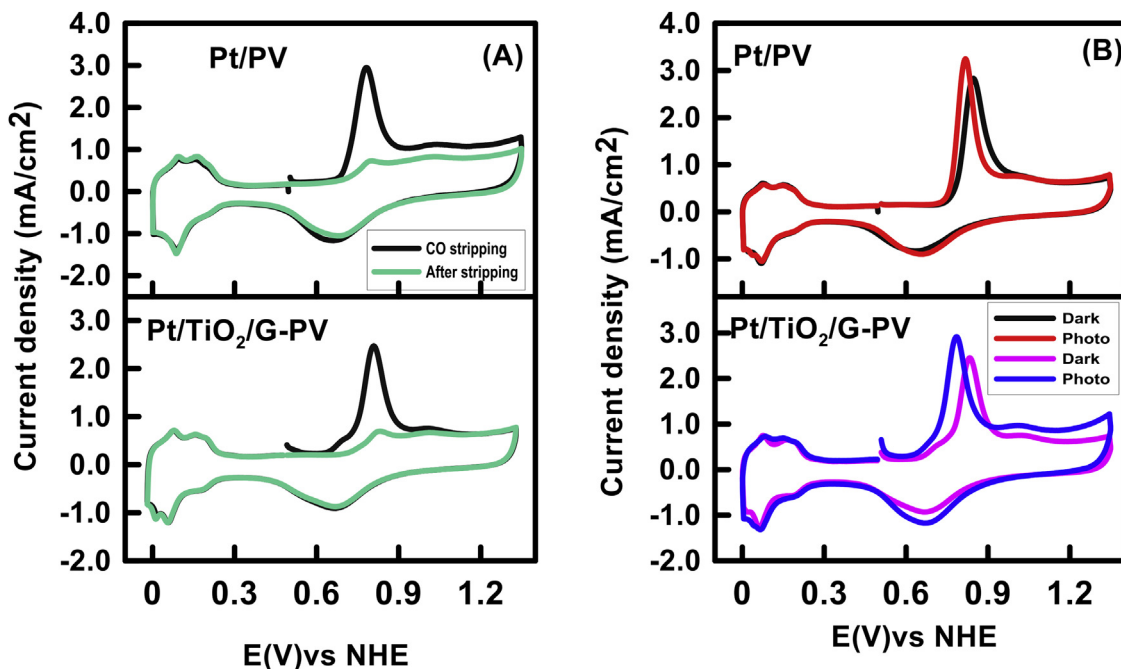


Fig. 12. (A) CO oxidation and stripping without illumination and (B) CO oxidation with and without illumination in 0.5 M H_2SO_4 solution at a scan rate of 50 mV/s and 25 °C. Currents normalized by glassy carbon electrode area = 0.196 cm^2 .

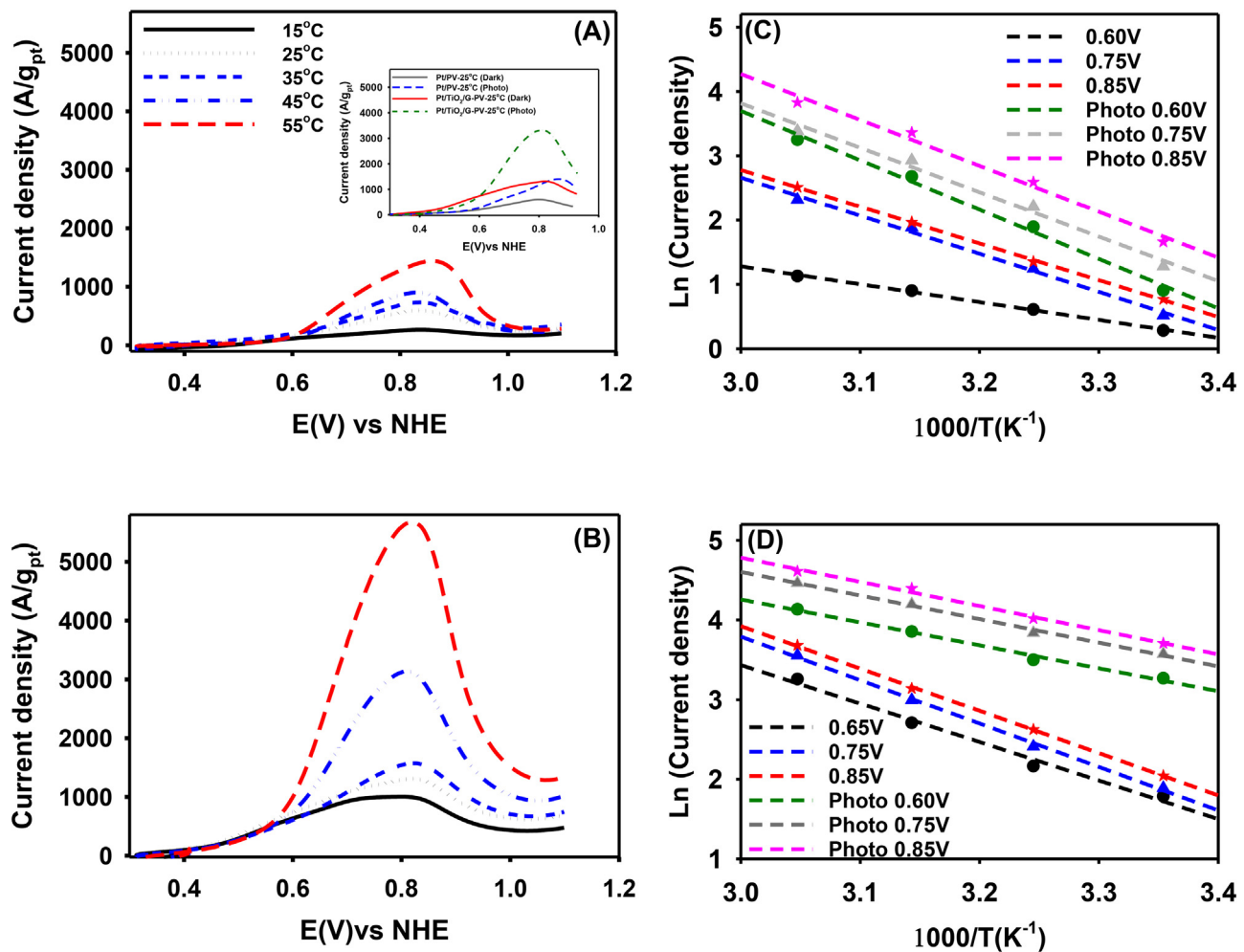


Fig. 13. Methanol oxidation on platinized supports (A) Pt/PV and (B) Pt/TiO₂/G-PV catalysts at different temperature without irradiation in nitrogen saturated 0.5 M CH₃OH + 0.5 M H₂SO₄ solution at 50 mV/s. Inset show methanol oxidation currents with and without irradiation at 25 °C. Corresponding Arrhenius plots of methanol oxidation at various temperatures with and without illumination for (C) Pt/PV and (D) Pt/TiO₂/G-PV catalysts.

Table 4

Activation energies (E_a) obtained from methanol oxidation at differential potentials for Pt/PV and Pt/TiO₂/G-PV catalysts with and without illumination.

Catalyst	E(V) vs NHE	Slope (E_a^{app}/R)	E_a^{app} (Dark) (kJ/mol)	E_a^{app} (Photo) (kJ/mol)
Pt/PV	0.60	6291	52.3	42.0
	0.75	8552	71.1	43.4
	0.85	8780	73.0	49.7
	0.60	5930	49.3	21.4
Pt/TiO ₂ /G-PV	0.75	6303	52.4	22.4
	0.85	6351	52.8	25.3

significant different; 73.0 and 52.8 kJ/mol for Pt/PV and Pt/TiO₂/G-PV, respectively. With illumination, E_a^{app} values obtained for Pt/PV and Pt/TiO₂/G-PV are in the order of 49.7 and 25.2 kJ/mol, respectively. This corresponds to 32% reduction in E_a^{app} in the case of the Pt/PV, and a 52% reduction in the case of Pt/TiO₂/G-PV. While heating of the electrode surface upon irradiation cannot be totally discarded, the significant different between samples with and without TiO₂, reinforces the idea that the observed enhancement is mostly due to a photocatalytic effect on the MOR kinetics. In this work, the obtained E_a^{app} values fall within the activation energy reported in the literature that varies from 16 to 95 kJ/mol depending on the test condition [54,55].

Based on the overall results, the improvement observed on the MOR on Pt/TiO₂/G-PV without illumination can only be due to two

main factors: (i) the oxophilic nature of TiO₂ NPs in the catalyst layer. The presence of –OH groups and other oxygen-containing species can facilitate the conversion of adsorbed CO species on Pt to CO₂ during methanol oxidation and (ii) the interaction between the PtNPs and TiO₂ NPs that can reduce the electron density of the d band of Pt with a consequently weakening of the binding energy between CO and Pt atoms, and making them easier to oxidize [56,57].

Moreover, we observed that the electrocatalytic performances of Pt/PV, as well as TiO₂ modified catalyst (Pt/TiO₂/G-PV) for the oxidation of methanol, are distinctly improved with illumination. As described earlier, this photo enhancement on Pt/PV catalyst may be ascribed to the plasmonic effect of PtNPs under illumination, with resulting charge carriers that eventually promote the oxi-

dation of methanol molecules. On the other hand, the methanol oxidation current on the Pt/TiO₂/G-PV electrode can be enhanced by several different modes: (i) electron-holes pair created on the TiO₂NPs surface during illumination that could independently oxidize methanol and produce a photocurrent by absorption of UV light. The energy of the TiO₂- valence band (VB) would easily allow the oxidation of methanol to an hydroxymethyl radicals, which can donate an electron to the conduction band (CB) of the semiconductor with the formation of formaldehyde, which can subsequently be converted to CO₂ [54]; (ii) the surface area of the Pt catalyst layer may be altered through electron-hole pairs induced under UV-vis illumination with an increase in methanol oxidation current [28]; and (iii) a current produced through a synergistic effect of the catalyst components, Pt, C and porous TiO₂ NPs under illumination which may result in a strong photoabsorption capacity [58,59].

Even though TiO₂ has a cooperative effect under illumination, leading to a much higher photocurrent on Pt/TiO₂/G-PV, similar charge transfer resistances were obtained for catalysts with and without TiO₂ under illumination.

4. Conclusions

In conclusion, we have evaluated performances of in-house catalysts Pt/PV and Pt/TiO₂/G-PV catalysts toward methanol oxidation reaction (MOR). The method used to prepare the Pt/TiO₂/G-PV composite catalyst as described in ref. 33 results in materials with a higher electrocatalytic activity than Pt/PV catalyst in the absence of illumination due to strong metal-support interaction. This improved performance is consistent with an observed negative shift in onset potential of CO oxidation on Pt/TiO₂/G-PV. With illumination, higher methanol oxidation currents are observed on these electrodes even in the absence of TiO₂ NPs.

Pt/PV show moderate enhancement in catalytic activity under illumination ($I_{\text{peak, illumination}} - I_{\text{peak, dark}}) * 100 / I_{\text{peak, dark}} \sim 100\%$) that can be attributed to a significant reduction in the charge transfer resistance (Rct) when the electrode is illuminated (635 Ω (dark) vs 84 Ω (illumination)) as determined by electrochemical impedance spectroscopy (EIS). The photo enhancement observed in the case of PtNPs deposited on TiO₂/G-PV is more impressive, ($I_{\text{peak, illumination}} - I_{\text{peak, dark}}) * 100 / I_{\text{peak, dark}} \sim 171\%$) even though the change in the Rct (185 Ω vs. 99 Ω) is not as pronounced as in the Pt/PV sample. Illumination leads to a reduction in the onset potential of ca. 40–50 mV for each catalyst, indicating that it does indeed alter energetic around CO removal.

This photo-assisted electrocatalytic process could remarkably enhance the oxidation efficiency toward methanol oxidation and can be utilized in outdoor fixtures where single stack cells can be spread to capture sunlight. Taking into account the engineering design constraint of fuel cell stack illumination, these electrode materials can be used as a tool to design disposable and portable electrochemical sensors for environmental monitoring such as water quality tests, organic compound analyses, heavy metals detection and gas pollutants. This light sensitive electrode can as well provide a breakthrough in developing a liquid methanol concentration sensor. Future work will involve further probing of the role of the PtNP by manipulating Pt surface area and examining its influence on the extent of photo-enhancement. This can be accomplished *in situ* by employing a typical accelerated stress test (AST) protocol that will cause the dissolution/aggregation of PtNPs [60,61]. In addition, more studies will be required to quantify individual contributions to the observed photocurrent from photo-generated holes in TiO₂ electrode and electron-hole pairs produced by the synergistic effect of the catalyst components.

Acknowledgements

This work was supported by the Natural Sciences and Engineering Research Council (NSERC) of Canada through the Discovery Grant program and the Faculty of Science at the University of Ontario Institute of Technology. We are grateful to Dr. Rana Sodhi (University of Toronto) and Dr. Lei Zhang (University of Waterloo) for assistance with XPS and TEM measurements. We also thank Dr. Andreas Korinek from the Canadian Centre for Electron Microscopy (McMaster University) for assistance with Electron microscopy (HR-TEM).

Appendix A. Supplementary data

Supplementary data associated with this article can be found, in the online version, at <http://dx.doi.org/10.1016/j.apcatb.2017.03.027>.

References

- [1] H.R. Corti, E.R. Gonzalez, *Direct Alcohol Fuel Cells*, Springer, Netherlands, 2014, pp. 1–32.
- [2] Kruth A., Todd M. J., Macphee D. E., Wells R. P. K. (2011). Fuel cell: Google Patents.
- [3] J. Ryu, W. Choi, Environ. Sci. Technol. 42 (1) (2008) 294–300.
- [4] D. Li, H. Haneda, S. Hishita, N. Ohashi, Chem. Mater. 17 (10) (2005) 2596–2602.
- [5] R.G. Freitas, M.C.D. Santos, R.T.S. Oliveira, L.O.S. Bulhões, E.C. Pereira, J. Power Sources 158 (1) (2006) 164–168.
- [6] X. Zhou, X. Xie, M. Ishikawa, Adv. Mater. Res. 347 (2012) 3281–3285.
- [7] W. Qian, D.P. Wilkinson, J. Shen, H. Wang, J. Zhang, J. Power Sources 154 (1) (2006) 202–213.
- [8] H. Fukunaga, T. Ishida, N. Teranishi, C. Arai, K. Yamada, Electrochim. Acta 49 (13) (2004) 2123–2129.
- [9] Y.X. Chen, A. Miki, S. Ye, H. Sakai, M. Osawa, J. Am. Chem. 125 (13) (2003) 3680–3681.
- [10] R. Parsons, T. VanderNoot, J. Electroanal. Chem. 257 (1) (1988) 9–45.
- [11] Z. Cui, C.M. Li, S.P. Jiang, Phys. Chem. Chem. Phys. 13 (36) (2011) 16349–16357.
- [12] Y.W. Lee, A.R. Ko, S.B. Han, H.S. Kim, K.W. Park, Phys. Chem. Chem. Phys. 13 (13) (2011) 5569–5572.
- [13] X.W. Yu, S.Y. Ye, J. Power Sources 172 (2007) 145–154.
- [14] Z. Xiao, M. Yin, L. Ma, L. Liang, C. Liu, J. Liao, T. Lu, W. Xing, Energy Environ. Sci. 4 (8) (2011) 2736–2753.
- [15] M. Cao, D. Wu, R. Cao, ChemCatChem 6 (1) (2014) 26–45.
- [16] H. Huang, X. Wang, J. Mater. Chem. A 2 (18) (2014) 6266–6291.
- [17] Z. Yao, M. Zhu, F. Jiang, Y. Du, C. Wang, P. Yang, J. Mater. Chem. 22 (27) (2012) 13707–13713.
- [18] Chen J.M., Sarma L.S., Chen C.H., Chen M.Y., Shih S.C., Wang G.R., Hwang B.J., J. Power Sources 159 (2006) 29–33.
- [19] M. Hepel, I. Kumarihamy, C.J. Zhong, Electrochim. Commun. 8 (9) (2006) 1439–1444.
- [20] R.A.M. Esfahani, A.H. MonteverdeVidela, S. Vankova, S. Specchia, Int. J. Hydrogen Energy 40 (42) (2015) 14529–14539.
- [21] Y.Q. Wang, Z.D. Wei, B. Gao, X.Q. Qi, L. Li, Q. Zhang, M.R. Xia, J. Power Sources 196 (3) (2011) 1132–1135.
- [22] L. Ye, Z. Li, L. Zhang, F. Lei, S. Lin, J. Colloid Interf. Sci. 433 (2014) 156–162.
- [23] K. Vinodgopal, S. Hotchandani, P.V. Kamat, J. Phys. Chem. 97 (35) (1993) 9040–9044.
- [24] X. Li, Z. Zhuang, W. Li, H. Pan, Appl. Catal. A: Gen. 429 (2012) 31–38.
- [25] A.W. Xu, Y. Gao, H.Q. Liu, J. Catal. 207 (2) (2002) 151–157.
- [26] B.Y. Xia, H.B. Wu, J.S. Chen, Z. Wang, X. Wang, X.W.D. Lou, Phys. Chem. Chem. Phys. 14 (2) (2012) 473–476.
- [27] C. Zhai, M. Zhu, F. Ren, Z. Yao, Y. Du, P. Yang, J. Hazard. Mater. 263 (2013) 291–298.
- [28] P. Li, Z.P. Li, B.H. Liu, J. Power Sources 199 (2012) 146–149.
- [29] K. Fukutani, M.B. Song, Y. Murata, J. Chem. Phys. 103 (6) (1995) 2221–2228.
- [30] D.V. Arulmani, J.I. Eastcott, S.G. Mavilla, E.B. Easton, J. Power Sources 247 (2014) 890–895.
- [31] S. Linic, U. Aslam, C. Boerigter, M. Morabito, Nat. Mater. 14 (6) (2015) 567–576.
- [32] M.L. Brongersma, N.J. Halas, P. Nordlander, Nat. Nanotechnol. 10 (1) (2015) 25–34.
- [33] C. Odetola, E.B. Easton, L. Trevani, Int. J. Hydrogen Energy 41 (19) (2016) 8199–8208.
- [34] C. Odetola, L. Trevani, E.B. Easton, J. Power Sources 294 (2015) 254–263.
- [35] K. Han, J.S. Lee, S.O. Park, S.W. Lee, Y.W. Park, H. Kim, Electrochim. Acta 50 (2004) 791–794.
- [36] D. Sebastian, I. Suelves, R. Moliner, M.J. Lazaro, Carbon 48 (2010) 4421–4431.
- [37] J.H. Park, S. Kim, A.J. Bard, Nano Lett. 6 (2006) 24–28.
- [38] S. Bonanni, K. Ait-Mansour, H. Brune, W. Harbich, ACS Catal. 1 (4) (2011) 385–389.

- [39] J.A. Horsley, *J. Am. Chem. Soc.* 101 (11) (1979) 2870–2874.
- [40] Z. Awaludin, M. Suzuki, J. Masud, T. Okajima, T. Ohsaka, *J. Phys. Chem. C* 115 (51) (2011) 25557–25567.
- [41] Z. Awaludin, J.G.S. Moo, T. Okajima, T. Ohsaka, *J. Mater. Chem. C* 1 (46) (2013) 14754–14765.
- [42] G. Selvarani, S. Maheswari, P. Sridhar, S. Pitchumani, A.K. Shukla, *J. Electrochem. Soc.* 156 (11) (2009) B1354–B1360.
- [43] C.S. Chen, F.M. Pan, *Appl. Catal., B: Environ.* 91 (3–4) (2009) 663–669.
- [44] N.M. Marković, P.N. Ross, *Surf. Sci. Rep.* 45 (4) (2002) 117–229.
- [45] W. Li, Y. Bai, F. Li, C. Liu, K.Y. Chan, X. Feng, X. Lu, *J. Mater. Chem.* 22 (9) (2012) 4025–4031.
- [46] C. Wang, F. Jiang, R. Yue, H. Wang, Y. Du, *J. Solid State Electrochem.* 18 (2) (2014) 515–522.
- [47] G. Wu, L. Li, B.Q. Xu, *Electrochim. Acta* 50 (1) (2004) 1–10.
- [48] F. Seland, R. Tunold, D.A. Harrington, *Electrochim. Acta* 51 (18) (2006) 3827–3840.
- [49] B. Hirschorn, M.E. Orazem, B. Tribollet, V. Vivier, I. Frateur, M. Musiani, *J. Electrochem. Soc.* 157 (12) (2010) C452–C457.
- [50] B. Ma, J. Bai, L. Dong, *J. Solid State Electrochem.* 17 (11) (2013) 2783–2788.
- [51] I.M. Hsing, X. Wang, Y.J. Leng, *J. Electrochim. Soc.* 149 (5) (2002) A615–A621.
- [52] J. Newman, K.E. Thomas-Alyea, *Electrochemical Systems*, 3rd Edition, Wiley Interscience, 2004.
- [53] C. Clavero, *Nat. Photonics* 8 (2) (2014) 95–103.
- [54] Z. Jusys, J. Kaiser, R.J. Behm, *Electrochim. Acta* 47 (22) (2002) 3693–3706.
- [55] J.L. Cohen, D.J. Volpe, H.D. Abruna, *Phys. Chem. Chem. Phys.* 9 (2007) 49–77.
- [56] H.A. Gasteiger, N. Markovic, P.N. Ross, E.J. Cairns, *J. Electrochim. Soc.* 141 (1994) 1795–1803.
- [57] I. Fampiou, A. Ramasubramaniam, *J. Phys. Chem. C* 39 (2013) 19927–19933.
- [58] S.J. Yoo, K.S. Lee, Y.H. Cho, S.K. Kim, T.H. Lim, Y.E. Sung, *Electrocatalysis* 2 (4) (2011) 297–306.
- [59] C. Colbeau-Justin, M. Kunst, D. Huguenin, *J. Mater. Sci.* 38 (11) (2003) 2429–2437.
- [60] A.M. Eppler, I.M. Ballard, J. Nelson, *Physica E* 14 (1) (2002) 197–202.
- [61] F.S. Saleh, E.B. Easton, *J. Electrochim. Soc.* 159 (2012) B546–B553.
- [62] O.R. O'Rian, F.S. Saleh, E.B. Easton, *ECS Trans.* 61 (23) (2014) 25–32.

Further reading